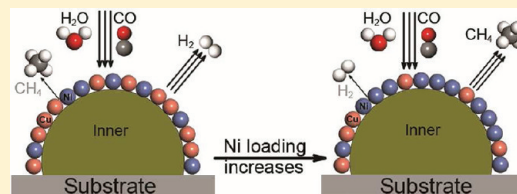


Catalytic Reactivity of CuNi Alloys toward H₂O and CO Dissociation for an Efficient Water–Gas Shift: A DFT Study

Li-Yong Gan,^{†,‡} Ren-Yu Tian,[†] Xiao-Bao Yang,[†] Hong-Duo Lu,[†] and Yu-Jun Zhao^{*,†,‡}[†]Department of Physics and [‡]State Key Laboratory of Luminescent Materials and Devices, South China University of Technology, Guangzhou 510640, P. R. China

ABSTRACT: Density functional theory (DFT) calculations are employed to study H₂O and CO dissociations on a set of CuNi bimetallic surfaces aiming at exploring the optimal Ni ensemble on Cu(111) for an efficient water–gas shift (WGS) process, i.e., splitting H₂O with high reactivity and avoiding CO activation. We found that Ni additives in the Cu(111) surface layer including a Ni monomer can remarkably enhance water splitting. Meanwhile, H₂O dissociation barriers (E_{act}) are strongly correlated with the H adsorption energies (E_{ad}): the larger E_{ad} , the smaller E_{act} . Moreover, H₂O dissociation may be more practical via the dissociated H* rather than OH closing to Ni atoms. For the scission of the C–O bond, the process is unfavorable on Ni monomers, though it is obviously promoted on Ni dimers, trimers, and other ensembles with higher Ni content. It is deduced that the selectivity of the Cu–Ni bimetallic catalysts toward WGS would decrease with increasing Ni concentration. These findings suggest that the bimetallic CuNi catalysts with highly dispersed Ni ensembles containing lower Ni concentration should exhibit high performance for the WGS process.



1. INTRODUCTION

The water–gas shift (WGS) reaction is an important chemical process for maximizing hydrogen production and removing residual CO in H₂ fuel cell systems and thus attracting increasing interest in heterogeneous catalysis.^{1–10} The reaction, CO + H₂O ↔ CO₂ + H₂, is a little exothermic at room temperature, yielding ~41 kJ/mol. Therefore, low reaction temperatures favor the equilibrium forward, while high ones are required to accelerate the reaction rate. To reconcile the contradiction, a two-step WGS reactor is employed in large-scale industrial plants: high-temperature shift (Fe₂O₃/Cr₂O₄) and low-temperature shift (Cu/ZnO/Al₂O₃).¹¹ However, such a process is complicated with multiple activation steps and thus not a ready solution for small-scale applications, such as hydrogen-fuel-cell-driven autos.¹² For the low-temperature copper-based WGS catalysts, the opening step, H abstraction from H₂O, is found to be the rate-limiting step for the entire WGS process.³ Consequently, it is of crucial importance to develop new WGS catalysts with high activity toward H₂O dissociation at low temperatures.

The catalytic performances of bimetallic alloys are often superior to those of pure metals^{13,14} and thus provide a new field for catalyst design. Their higher flexibility in chemical composition and interatomic arrangement compared to pure metals can open new reaction pathway and hence improve both the reactivity and selectivity of catalysts. A report⁴ from Knudsen and co-workers has shown that the Cu/Pt near-surface alloy is a promising candidate for improving low-temperature WGS reactivity. However, the reaction barrier of H₂O splitting on the alloy is still as high as that on Cu.⁴

Recently, Schumacher and co-workers¹⁵ employed a microkinetic model based on a redox mechanism to study the trend of

low-temperature WGS reactivity on a series of transition metals (TMs) and suggested that the catalytic reactivity of Cu and Ni may be superior to other TMs. Meanwhile, through Reaction Route Graph Analysis, Callaghan et al.¹⁶ also concluded that Cu and Ni are the most promising metal components for the WGS with respect to other TMs. Furthermore, Ni is more reactive toward H₂O than Cu in the WGS process.² Intuitively, introducing the Ni component to the Cu-based catalysts may lower the barrier of H₂O splitting and ultimately accelerate the WGS process at low temperatures.

Several experimental studies have been carried out to compare the catalytic activity and selectivity of Cu–Ni bimetallic systems with those of monometallic Cu or Ni catalysts.^{17–22} Adding Cu into Ni catalysts in the ethanol steam reforming reaction not only reduces CO generation but also improves the resistance to coke formation.¹⁸ The additive of Cu into Ni/SiO₂ can improve the selectivity of the vinyl chloride monomer effectively.¹⁹ Huang et al.²¹ studied the weighting variation of WGS in steam reforming of methane as a function of Ni–Cu ratios and concluded that the addition of Cu into a Ni catalyst could enhance the WGS activity. More recently, Lin and co-workers²² systematically investigated the WGS over a series of Ni, Cu, and Cu–Ni bimetallic catalysts with different Cu/Ni ratios. They found that increasing Ni loading in Cu could enhance the WGS reactivity but meanwhile decrease the selectivity; namely, the undesirable methane yield increased.

Received: August 23, 2011

Revised: December 7, 2011

Published: December 12, 2011

Unfortunately, on a microscopic level, the effect of the Cu–Ni alloy on the activity and selectivity of WGS is still not well determined, which might raise some corresponding questions such as: (1) How does Ni addition enhance the WGS activity? (2) What is the optimal CuNi ensemble for WGS? Hence, we herein carry out a comprehensive density functional theory (DFT) study to systematically investigate the effects of different Ni ensembles (monomer, dimer, trimer, and pseudomonolayer) incorporation into a Cu(111) catalyst on the rate-limiting step of WGS³ to assess the activity of CuNi toward WGS. This is based on the assumption that a small amount of Ni in Cu catalysts would not alter the entire WGS process. Meanwhile, since CO activation on the catalysts is essential to the formation of CH₄ and other hydrocarbons^{23–26} (so-called synthesis gas conversion), CO activation on several selected Cu–Ni bimetallic surfaces is thus comparatively studied to explore the optimal ensemble with high reactivity toward water splitting and low reactivity toward CO activation. We show that Ni ensembles with lower Ni concentration in Cu–Ni catalysts may maintain the C–O scission barrier and thus avoid the undesired methanation side reaction.

2. COMPUTATIONAL DETAILS

This work is conducted by the Vienna Ab Initio Simulation Package (VASP)^{27–30} with the frozen-core projector-augmented-wave (PAW) method.^{31,32} The spin-polarized Perdew–Wang (PW91) generalized gradient approximation (GGA)^{33,34} functional was employed for the exchange–correlation energy. A cutoff energy of 500 eV was employed for the plane-wave expansion. A $p(3 \times 3)$ lateral super cell is used with a $5 \times 5 \times 1$ γ -centered k -point mesh throughout the study. The surfaces are modeled with a five-layer slab with a vacuum thickness of 15 Å. The CuNi bimetallic systems are designed with Cu atoms in the first or second layer substituted by Ni atoms, as shown in Figure 1. The adsorbed species are put on one side of the slab. The positions of all atoms except those in the two bottommost layers are fully relaxed until the residual forces of each relaxed ion are less than 0.03 eV/Å. The lattice constants of Cu and Ni bulk are fully optimized to 3.64 and 3.52 Å, respectively, in good agreement with the experimental values of 3.61 and 3.52 Å.³⁵ The adsorption energies (or binding energies) of X (X = H₂O, OH, H, CO, C, and O) on metal surfaces are defined as

$$E_{\text{ad}} = - (E_{\text{tot}}^{\text{X/M}(111)} - E_{\text{tot}}^{\text{M}(111)} - E_{\text{tot}}^{\text{X}})$$

where $E_{\text{tot}}^{\text{X/M}(111)}$, $E_{\text{tot}}^{\text{M}(111)}$, and $E_{\text{tot}}^{\text{X}}$ are the total energies of X (X = H₂O, OH, H, CO, C, and O) adsorbed mono- and bimetallic surfaces, clean metal surfaces, and X in gas phases, respectively.

Energy barriers and minimum energy paths (MEPs) of H₂O and CO dissociation have been computed using the climbing-image nudged elastic band (CI-NEB).³⁶ After standard transition state (TS) searching, the TS is further optimized by the quasi-Newton method until the residual forces are less than 0.03 eV/Å.

3. RESULTS AND DISCUSSIONS

3.1. H₂O Dissociation on Mono- and Bimetallic Surfaces.

In this section, H₂O dissociation on the mono- and bimetallic surface is comparatively studied to investigate the effect of Ni additives. The surfaces are divided into five groups (groups 2–5 are shown in Figure 1). Group 1: monometallic Cu(111) and

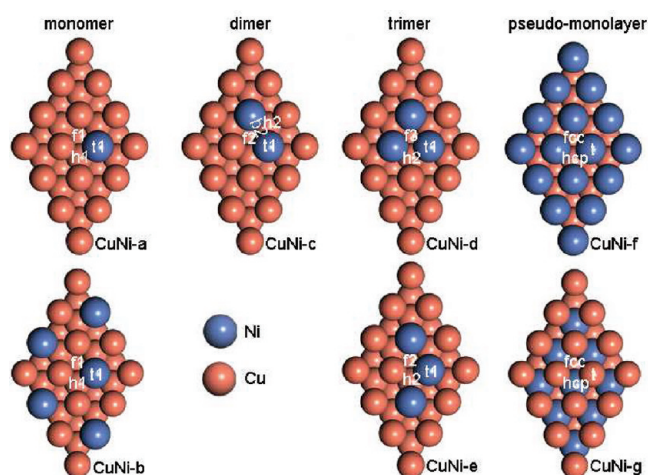


Figure 1. Unit cell of CuNi(111) surfaces with different Ni ensembles. In (a)–(e), Ni atoms substitute for Cu atoms in the surface layer. The adsorption sites on Ni ensembles are marked with letters and numbers: t, b, f, and h represent the atop, bridge, fcc, and hcp sites, respectively; 1, 2, and 3 indicate sites coordinated with one, two, and three Ni atoms, respectively. In CuNi-f and CuNi-g, the first and second Cu layers are replaced by a Ni pseudomonolayer, respectively. The bimetallic CuNi(111) surfaces are divided into four groups and arranged in four columns to guide the eye.

Ni(111); group 2: CuNi bimetallic surfaces with Ni monomer, CuNi-a and CuNi-b; group 3: CuNi bimetallic surfaces with Ni dimer, CuNi-c; group 4: CuNi bimetallic surfaces with Ni trimer, CuNi-d (trimer- α) and CuNi-e (trimer- β); group 5: CuNi bimetallic surfaces with a Ni pseudomonolayer, CuNi-f and CuNi-g. It has been experimentally shown^{22,37} that Ni atoms prefer to interact with Cu to form Cu–Ni alloys rather than the oxide support at low Ni concentration. Namely, the oxide support may be almost unchanged at low Ni loading. Thus, the possible role of oxide supports was not taken into account in the present work, but it may be important for some catalysts.^{9,10} The calculated surface free energy of Ni(111) is 0.64 eV/atom, larger than the value of Cu(111), 0.45 eV/atom, indicating that Ni impurities are prone to staying in the bulk in CuNi alloys under ultrahigh vacuum (UHV). At appropriate high temperature, Ni atoms can diffuse outward. In addition, some adsorbates (e.g., CO and O) can also induce Ni diffusion out of surface. The energy difference between a Ni atom incorporated in the surface and a subsurface layer ($\Delta E = E_{\text{surf}} - E_{\text{sub}}$) without any adsorbates is 0.21 eV, while it changes to -0.66 eV if the surface is covered by 0.11 ML CO [i.e., one CO in a (3×3) supercell]. Therefore, the presence of Ni atoms in the surface layer can be expected under the operating condition in WGS reaction.

3.1.1. H₂O Dissociation on Monometallic Cu(111) and Ni(111). First, the adsorption of the reactant and products for H₂O dissociation on the two pure surfaces is investigated as a test calculation. The most stable configurations for H₂O adsorptions on the two surfaces both correspond to H₂O at the top sites with the molecular plane almost parallel to the surfaces, shown in Figure 2(h) and (i). The binding energies are 0.20 and 0.31 eV, respectively. The H–O–H angles are 105.5° and 106.0°, respectively, and the O–H bond lengths are both 0.98 Å, which are similar to the values of H₂O in the gas phase, 103.8° and 0.97 Å, indicative of the weak interactions. Accordingly, these configurations are subsequently chosen as the initial states (ISs) for the

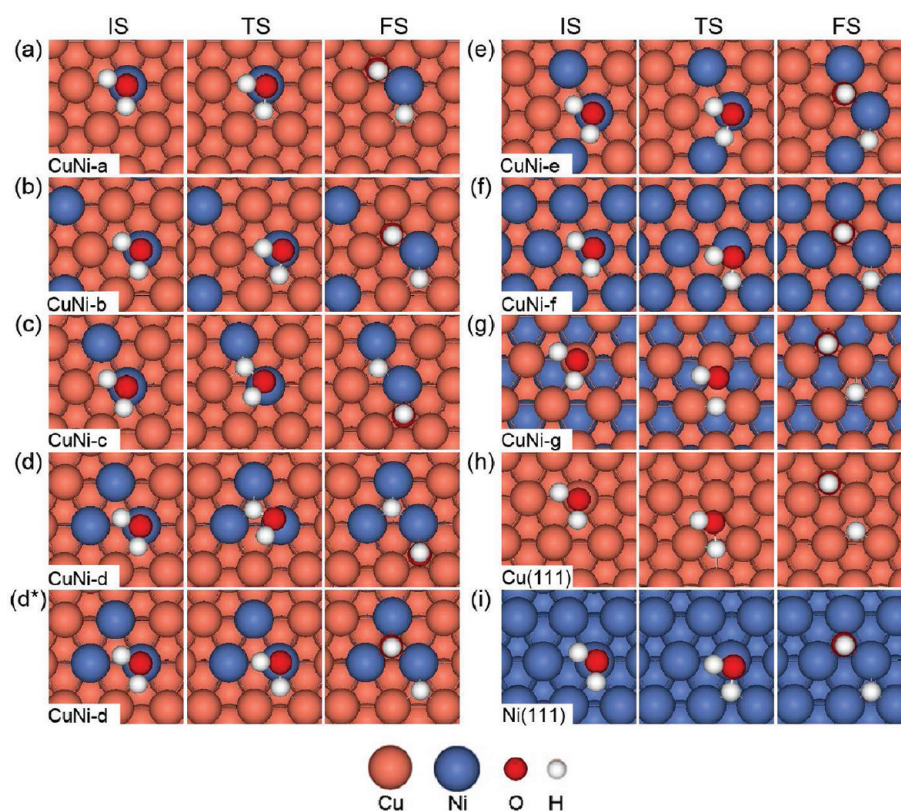


Figure 2. Geometrical structures of IS, TS, and FS of the $\text{H}_2\text{O}^* + * \rightarrow \text{H}^* + \text{OH}^*$ reaction on bimetallic CuNi and pure Cu(111) and Ni(111).

Table 1. Adsorption Energies, E_{ad} (eV), of H_2O , H, along with OH, and Co-Adsorption Energies of H and OH on Mono- and Bimetallic Surfaces^a

surfaces	$E_{\text{ad}}(\text{H}_2\text{O})$	$E_{\text{ad}}(\text{H})$	$E_{\text{ad}}(\text{OH})$	$E_{\text{ad}}(\text{H} + \text{OH})$
Cu(111)	0.20(t)	2.48(f)/2.49(h)	3.24(f)	5.66(f+f)
CuNi-a	0.32(t1)	2.68(f1)/2.70(h1)	3.29(f1)	5.90(f1+f1)
CuNi-b	0.30(t1)	2.68(f1)/2.69(h1)	3.23(f1)	5.84(f1+f1)
CuNi-c	0.31(t1)	2.82(f2)/2.83(h2)	3.45(f2)	6.13(f2+f1)
CuNi-d	0.32(t1)	2.96(f3)	3.63(f3)	6.27(f3+f1)
CuNi-e	0.31(t1)	2.82(f2)/2.83(h2)	3.43(f2)	6.25(f2+f2)
CuNi-f	0.30(t)	2.98(f)/2.96(h)	3.54(f)	6.50(f+f)
CuNi-g	0.24(t)	2.49(f)/2.48(h)	3.22(f)	5.71(f+f)
Ni(111)	0.31(t)	2.83(f)/2.82(h)	3.42(f)	6.18(f+f)

^a The adsorption sites in bold font are defined in Figure 1.

dissociation step. H atomic adsorption at the two 3-fold hollow sites (fcc and hcp) is more favorable with almost degenerated binding energies (E_{ad}) (cf. Table 1): 2.48/2.49 eV and 2.83/2.82 eV at fcc/hcp on Cu(111) and Ni(111), respectively. OH adsorption at the fcc is more favorable with O–H perpendicular to the surfaces. The values of E_{ad} are 3.24 and 3.42 eV, respectively. The coadsorption of the two products is calculated with H and OH at two adjacent fcc sites. The binding energy on Cu(111) is smaller than that on Ni(111), 5.66 vs 6.18 eV. A very weak repulsion can be extracted between the two coadsorbates, 0.06 and 0.03 eV, respectively. This is because H and OH bond directly to the same metal atom [seen in Figure 2(h) and (i)], giving rise to a repulsion due to the bonding competition. The coadsorption configurations are chosen as the final states (FSs).

Table 2. Activation Barrier Energies ($E_{\text{act}} = E_{\text{TS}} - E_{\text{IS}}$), Reaction Energies ($\Delta E = E_{\text{FS}} - E_{\text{IS}}$), and Geometrical Parameters of Transition States for H_2O Dissociation on Mono- and Bimetallic Surfaces^a

surfaces	E_{act} (eV)	ΔE (eV)	$d_{\text{H}^*-\text{O}}$ (Å)	$d_{\text{H}-\text{O}}$ (Å)
Cu(111)	1.31	0.11	1.48	0.98
CuNi-a	1.01	0.00	1.58	0.98
CuNi-b	1.01	0.09	1.56	0.98
CuNi-c	0.83	−0.24	1.53	0.98
CuNi-d	0.79	−0.38	1.54	0.98
CuNi-e	0.83	−0.37	1.53	0.98
CuNi-f	0.77	−0.65	1.51	0.98
CuNi-g	1.24	0.10	1.61	0.98
Ni(111)	0.90	−0.29	1.54	0.98

^a $d_{\text{H}^*-\text{O}}$, bond length between dissociated H^* and O; $d_{\text{H}-\text{O}}$, bond length between H and O in OH.

These results are in good agreement with previous studies,^{2,3,38–40} confirming that the accuracy of the present work is sufficiently adequate.

Upon the basis of the above results, the reaction for H_2O dissociation on Cu(111) and Ni(111) is calculated by CI-NEB.³⁶ The activation barriers ($E_{\text{act}} = E_{\text{TS}} - E_{\text{IS}}$) and the reaction energies ($\Delta E = E_{\text{FS}} - E_{\text{IS}}$) relative to ISs as well as the geometrical parameters of the transition states (TSs) are listed in Table 2. The reaction is slightly thermodynamically unfavorable on Cu with a ΔE of 0.11 eV and favorable on Ni(111) ($\Delta E = -0.29$ eV). The calculated barrier is 1.31 eV on Cu, higher than that on Ni, 0.90 eV. As shown in Figure 2(h), the TS on Cu is

located with the dissociated H atom (hereafter denoted as H^{*}) at a bridge-like site and OH near fcc. The distance between the H^{*} and O atom is 1.48 Å. The TS on Ni is somewhat different: OH is at an off-top site, while H^{*} is almost at an fcc site. The H^{*}–O distance is 1.54 Å. Our results are well consistent with earlier reports,^{2–4,40–42} while the E_{act} values slightly differ probably due to different cell size and pseudopotential choices.

3.1.2. H₂O Dissociation on Bimetallic CuNi(111). To investigate the effects of Ni incorporation into a Cu catalyst, water splitting on a set of CuNi bimetallic surfaces is studied, as shown in Figure 1. First, we systematically calculate the initial states, i.e., water adsorption on the bimetallic surfaces. On CuNi(111) with Ni atoms in the first layer, from CuNi-a to CuNi-f, H₂O adsorbs at the top of the Ni atom still with its plane almost parallel to the surfaces, seen in the first column of Figure 2. The bonding energies are all around 0.30 eV, and the O–Ni and O–H bond lengths are all 2.15 and 0.98 Å on each surface. The H–O–H angles range from 105° to 106°. These results are similar to those found on the pure Ni(111) surface. On CuNi-g, where Ni atoms are in the second layer, the results are close to those on Cu(111). In the following subsections, H and OH isolated adsorption and coadsorption, the reaction pathways, reaction energies, and barriers are calculated on the bimetallic CuNi surfaces. The promotional effects mentioned below are all referred to the results on pure Cu(111) unless otherwise stated.

3.1.2.1. On the Ni Monomer: CuNi-a and CuNi-b. The effects of a Ni monomer are investigated comparatively in two models: one with an isolated Ni monomer and the other with three nonadjacent Ni monomers in the $p(3 \times 3)$ cell [cf. Figure 1 (a) and (b)]. First, H and OH adsorption are calculated, and only the results of the respective most stable configuration are listed in Table 1. The adsorption energies of H at f1 and h1, where the Ni monomer is bonded, are almost the same on both surfaces and increased by ~0.20 eV in the presence of Ni. OH prefers to adsorb at f1 on CuNi-a and CuNi-b with E_{ad} almost unchanged. When H and OH coadsorb at two adjacent f1 sites, shown in the third column in Figure 2 (a) and (b), the E_{ad} are 5.90 and 5.84 eV, respectively, a little smaller than the summation of individual E_{ad} of H and OH. This suggests there is only a weak bonding competition, similar to the cases on Cu and Ni(111). Meanwhile, the values are also increased by about 0.20 eV since H adsorption is stabilized on the Ni monomer. The configurations are thus identified as the FSs for H₂O dissociation on CuNi-a and CuNi-b. The structures of the TS on both surfaces correspond to OH almost remaining at the atop site and the dissociated H^{*} moving toward the f1 site. The distances between H^{*} and O are 1.58 and 1.56 Å, respectively. The reaction on the Ni monomer is practically thermo-neutral (0 eV on CuNi-a and 0.09 eV on CuNi-b) with an activation energy of 1.01 eV on both surfaces.

3.1.2.2. On the Ni Dimer: CuNi-c. As shown in Table 1, H prefers the two hollow sites with two Ni atoms involved and gets close to the two Ni atoms. The adsorption energies are 2.82 eV at f2 and 2.83 eV at h2. The most energetically favorable site for OH adsorption is f2 with a value of 3.45 eV. Subsequently, two coadsorption configurations are considered: one with H at f2 and OH at the adjacent f1 [Figure 2(c)] and the other with OH at f2 and H at f1 reversely (not shown). The former is more stable with E_{ad} of 6.13 eV and therefore chosen as the FS for the H₂O splitting. As shown in Figure 2(c), the departing H^{*} is approaching a near-bridge site which is coordinated with two Ni atoms, and the OH is a little bit away from the Ni-top site in the TS. The H^{*}–O distance changes from 0.98 Å in IS to 1.53 Å in TS. The

reaction is exothermic by 0.24 eV, and the dissociative barrier is calculated to be 0.83 eV.

3.1.2.3. On the Ni Trimer: CuNi-d and CuNi-e. Two configurations are taken into account to explore the ensemble effects on H₂O dissociation on the Ni trimer, CuNi-d (trimer- α) and CuNi-e (trimer- β), shown in Figure 1 (d) and (e). The most energetically preferred site for either H or OH adsorption on CuNi-d is the 3-fold f3. The adsorption energies are 2.96 and 3.63 eV, respectively, which are much higher than those on the Ni monomer and dimer. Two reaction pathways are considered on trimer- α : H₂O(t) → H(f3) + OH(f1) [Figure 2(d)] and H₂O(t) → H(f1) + OH(f3) [Figure 2(d*)]. The two pathways have very similar reaction energies (–0.35 and –0.38 eV), but the former exhibits a smaller barrier than the latter (0.79 vs 1.01 eV). Thus, only the TS geometrical parameters of the former are listed in Table 2. In the corresponding TS structure, the dissociative H^{*} atom is close to the f3 with the OH slightly off its initial position. The H^{*}–O bond length is 1.54 Å. The lower barrier in the first pathway may be because the dissociated H^{*} atom overcomes the barrier via the near-f3 site (Ni-rich, more stable), instead of OH approaching f3. This can also be deduced from the results that the Ni-induced increment of H E_{ad} is more obvious than that of OH. As on trimer- β , the energies for H and OH individual adsorption are similar to that on the Ni dimer, while the coadsorption energy is a little higher (6.25 eV) with H and OH at two contiguous f2 sites [Figure 2(e)], which is selected as the FS for H₂O dissociation on trimer- β . As shown in Figure 2(e), the H^{*} is getting close to f2, while OH is slightly off its original site with a H^{*}–O bond length of 1.53 Å. The dissociation process is energetically favorable, –0.37 eV, and its energy barrier is found to be 0.83 eV.

3.1.2.4. On the Ni Pseudomonolayer: CuNi-f and CuNi-g. The alloy catalysts with a Ni monolayer in the first and second layers, seen in Figure 1(f) and (g), are contrastively studied to investigate how the subsurface Ni atoms affect H₂O dissociation. On CuNi-f, it can be seen from Table 1 that energies of H and OH adsorption at fcc are 2.98 and 3.54 eV, respectively, while the coadsorption energy with H and OH at two contiguous fcc sites (selected as FS) is 6.50 eV. The TS is similar to that on pure Ni(111) [Figure 2(f)] with the H^{*}–O distance of 1.51 Å. The reaction is exothermic by 0.65 eV with a barrier of 0.77 eV. On CuNi-g, E_{ad} of H and OH are calculated to be 2.49 and 3.22 eV, respectively, and E_{ad} of H and OH coadsorption is 5.71 eV. The TS structure is related to the dissociated H^{*} at a bridge site and OH off the top site ($d_{\text{H}^*-\text{O}} = 1.61$ Å), similar to that on Cu(111). The calculated reaction energy for H₂O* + * → H* + OH* on CuNi-g is 0.10 eV, a little bit endothermic, and the reaction barrier is 1.24 eV.

3.1.2.5. Comparison of H₂O Reactivity on Mono- And Bimetallic Surfaces. From Table 2, it can be seen that the dissociation barriers of H₂O on the bimetallic surfaces follow the trend of CuNi-g > CuNi-a = CuNi-b > CuNi-c = CuNi-e > CuNi-d ≈ CuNi-f. Additionally, the trend correlates well to the number of involved Ni atoms on which the reaction occurs. On CuNi-g, where Ni atoms are in the second layer and there are no direct Ni atoms participating in the reaction, the barrier is found comparable with that on pure Cu(111), indicating that the subsurface Ni has little effect on the reaction. On the Ni monomer (CuNi-a and CuNi-b), where the reaction processes over one Ni atom, the same barrier (1.01 eV) is obtained, which is 0.30 eV lower, suggesting that the incorporation of a Ni monomer into the Cu(111) surface layer enhances the catalytic activity toward

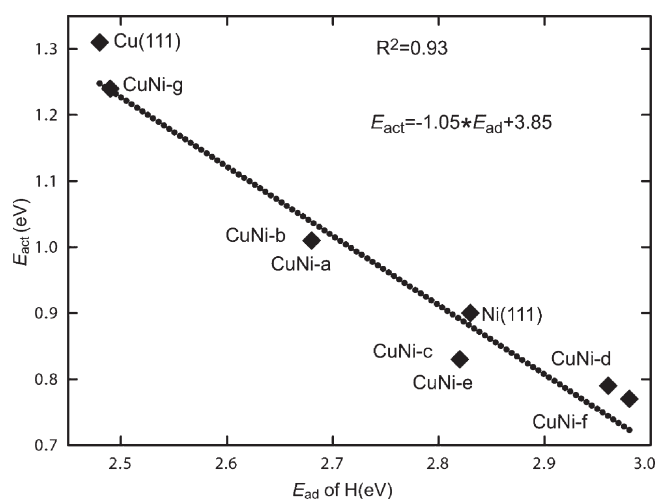


Figure 3. Relationship between H adsorption energies, E_{ad} , and the activation barriers for $\text{H}_2\text{O}^* + * \rightarrow \text{H}^* + \text{OH}^*$ reaction, E_{act} , on mono- and bimetallic surfaces.

water splitting and that the nonadjacent Ni atoms hardly affect the reaction. On the Ni dimer, CuNi-c, the reaction barrier is much smaller than that on the Ni monomer. Surprisingly, the H_2O dissociation barrier over Ni trimer- β is found to be the same as that on the Ni dimer though the FS is more stable, 6.25 versus 6.13 eV. In fact, the TS structures on the two ensembles are almost the same: H^* bonding to two Ni atoms and OH slightly off its initial site [cf. Figure 2(c) and (e)]. On CuNi-d and CuNi-f, the barriers are further reduced with H^* bonding to three Ni atoms in the TSs. It has been mentioned above that the barrier is calculated as high as that on the Ni monomer (1.01 eV) if the dissociation on CuNi-d proceeds via $\text{H}_2\text{O}(t) \rightarrow \text{H}(f1) + \text{OH}(f3)$, where the departing H^* atom is close to one Ni in the TS [Figure 2(d*)]. Additionally, all the TSs are late transition states with very large H^*-O distance. The configurations of OH in TSs (cf. Figure 2) are very close to each other: off-top adsorption. Moreover, it is found that Ni-induced increments of H adsorption on CuNi surfaces are more remarkable than those of H_2O and OH. These results together imply that the reaction barriers should be strongly dependent on the energetics of H adsorption. As a result, the dissociation barriers as a function of H adsorption energies are depicted in Figure 3, and a good linear correlation with $R^2 = 0.93$ is obtained. This verifies that the energy barriers are well correlated with H adsorption energies: the larger the adsorption energy the smaller the dissociation barrier. As for the reaction pathway, it is deduced that H_2O dissociation is more practical via the dissociated H^* rather than OH approaching Ni atoms. Moreover, we also analyzed the E_{act} for H_2O splitting as a function of the coadsorption energies of $\text{H} + \text{OH}$ (not shown). However, the correlation is not as good as that between E_{act} and E_{ad} of a single H atom. This may be ascribed to the fact that OH adsorption is not as sensitive as H to the structure of Ni ensembles, as shown in Table 1.

To rationalize the effects of bimetallic surfaces, the weighted d -band centers of the three metal atoms ready to bond with the H atom at the series of fcc sites (cf. Table 1 and Figure 1) are calculated by using the Pallassana model.⁴³ The correlation between the weighted d -band centers and H adsorption energies along with the activation barriers of H_2O dissociation are shown in Figure 4. It is obvious that the weighted d -band center

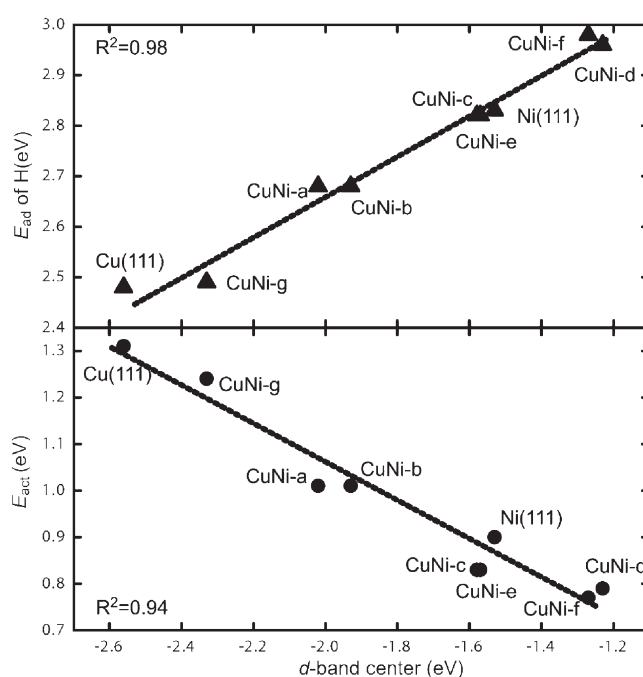


Figure 4. Correlations between E_{ad} (upper panel) as well as E_{act} (lower panel) and the weighted d -band center of the three metal atoms ready to bond with the H atom at a series of fcc sites (cf. Table 1 and Figure 1).

gradually gets close to the Fermi level (E_F) as the number of Ni atoms increases in the top layer from CuNi-a to CuNi-f and therefore results in higher H adsorption energies and lower reaction barriers on these surfaces. Conclusively, increasing Ni content in the surface layer can enhance the reactivity to H_2O splitting, accelerate the conversion of CO, and ultimately promote the WGS process.²²

3.2. CO Dissociation on Mono- and Bimetallic Surfaces. Ni is an effective catalyst for the methanation reaction,⁴⁴ and therefore the undesired CH_4 yield would increase as the additive of Ni content increases.²² On the basis of the H_2O dissociation trend above, CO dissociations on three representative surfaces, CuNi-a (monomer), CuNi-b (dimer), and CuNi-d (trimer- α), are studied in this section to check the activity of CuNi surfaces toward CO activation, which is required during the CH_4 formation. Meanwhile, CO dissociation on pure Cu(111) and Ni(111) is also calculated as a reference.

3.2.1. CO Dissociation on Monometallic Cu(111) and Ni(111). We first calculate the adsorption of the reactant (CO) and products (C and O) and the CO dissociation on two referred surfaces. The calculated adsorption energies are listed in Table 3, while the results of the dissociation are shown in Figure 5. On Cu(111), CO, C, and O all prefer the fcc site with the binding energies of 0.76, 4.88, and 5.03 eV, respectively. For C and O coadsorption at two adjacent fcc (initial setting), a large surface distortion is obtained after structural optimization: C bonding with four Cu atoms, as shown in Figure 5(c). The adsorption energy is 9.88 eV, only 0.03 eV smaller than the summation of C and O separate adsorption (9.91 eV), indicating that the distortion can effectively reduce the bonding competition between C and O. The calculated reaction pathway is thus from CO at fcc to the distorted coadsorption configuration. The process is endothermic with ΔE of 2.93 eV, and a very large barrier is obtained, 3.84 eV,

Table 3. Adsorption Energies, E_{ad} (eV), of CO, C, and O and the Coadsorption Energies of C and O on Mono- And Bimetallic Surfaces^a

system	E_{ad} (CO)	E_{ad} (C)	E_{ad} (O)	E_{ad} (C+O)
Cu(111)	0.76(f)	4.88(f)/4.82(h)	5.03(f)/4.94(h)	9.88(f+f)
CuNi-a	1.66(t1)	5.75(f1)/5.72(h1)	5.35(f1)/5.26(h1)	10.74(h1+f1)
CuNi-c	1.89(b2)	6.57(f2)/6.57(h2)	5.68(f2)/5.57(h2)	11.40(f2+f1)
CuNi-d	2.14(f3)	7.25(f3)	6.09(f3)	12.21(f3+f1)
Ni(111)	1.91(h)	6.86(f)/6.91(h)	5.74(f)/5.62(h)	12.47(h+f)

^aThe adsorption sites in bold font are defined in Figure 1.

suggesting that the C–O bond breaking on Cu is prohibited.⁴⁵ In the TS, the C atom almost sits at a bridge site, while O is close to an hcp (see Figure 5(d)). The C–O bond length is 2.00 Å, greatly elongated versus that in IS, 1.15 Å. On Ni(111), CO and C prefer hcp, while O prefers fcc with E_{ad} of 1.91, 6.91, and 5.74 eV, respectively. The coadsorption with C at hcp and O at fcc over a Ni atom [shown in Figure 5(e)] is weakly repulsive, 12.47 eV for coadsorption vs 12.65 eV for isolated adsorption. Subsequently, CO dissociation with C staying at hcp while O approaches fcc is calculated [Figure 5(d)] with a E_{act} of 2.92 eV. The TS corresponds to a C atom almost at an hcp and O at a bridge site. The C–O bond is stretched remarkably in comparison with that in the IS (1.48 vs 1.19 Å). Meanwhile, the transition states on both surfaces are late TSs and product-like. The adsorption energies along with the activation barriers for CO dissociation are in reasonable agreement with previous reports.^{25,46–49}

3.2.2. CO Dissociation on Bimetallic CuNi-a, CuNi-b, and CuNi-d. Before studying the effects of Ni ensembles on CO dissociation, CO as well as C and O adsorption was discussed, with the results listed in Table 3. Apparently, CO energetically prefers to bond with Ni atoms on the bimetallic surfaces: atop of the Ni atom (t1) on a Ni monomer; bridge site involved two Ni atoms (b2) on a Ni dimer; and hollow site contained three Ni (f3) on Ni trimer- α . These configurations are thus selected as ISs in the dissociation process. The adsorption energies are 1.66, 1.89, and 2.14 eV, respectively. The binding energy of CO on trimer- α is even larger than that on pure Ni(111). The interactions between CO and TMs are based on the donation from CO- 5σ states to TM- d states and back-donation from TM- d to the CO- $2\pi^*$ and can be well described by the d -band center model.^{50,51} As highly active Ni components incorporated into the Cu surface, the metal d -band gets close to E_{F} , and thus larger adsorption energies are obtained. Similarly, for isolated adsorption of C and O, the two adsorbates both tend to bond to Ni, especially the carbon atom. In addition, both C and O are not at the right center of the hollow site but closer to the Ni atoms in corresponding isolated adsorption configurations. The adsorption energies of the C atom are 5.75 eV (f1)/5.72 eV (h1) on the Ni monomer, 6.57 eV (f2)/6.57 eV (h2) on the Ni dimer, and 7.25 eV (f3) on Ni trimer- α . The O atom still favors fcc sites on each surface, 5.35 eV on CuNi-a, 5.68 eV on CuNi-c, and 6.09 eV on CuNi-d. The Ni addition induced enhancements of E_{ad} of C are more remarkable than those of O, suggesting C atomic adsorption is more sensitive to the structures of Ni ensembles. As a result, in the coadsorption of C and O (chosen as FSs on each surface), the more Ni atoms C bonds to, the larger the coadsorption energy is, as shown in Figure 5(a)–(c). On CuNi-a, the configuration is that C sits at an hcp and O at an fcc over the Ni

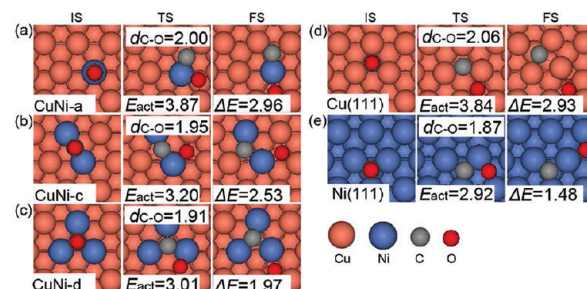


Figure 5. Geometrical structures of IS, TS, and FS of the $\text{CO}^* + * \rightarrow \text{C}^* + \text{O}^*$ reaction on Ni ensemble incorporation into Cu, Ni monomer (a), dimer (b), and trimer- α (c), as well as pure Cu(111) (d) and Ni(111) (e), marked with the activation barriers, E_{act} (eV), reaction energies, ΔE (eV), and the C–O bond lengths, $d_{\text{C-O}}$ (Å), in respective TSs correspondingly.

atom. On the Ni dimer and trimer- α , C is located at f2 on CuNi-c and f3 on CuNi-d, while O is at the adjacent f1 site. The coadsorption on the three bimetallic surfaces is weakly interacted, 10.74, 11.40, and 12.21 eV for coadsorption versus 11.07, 11.83, and 12.60 eV for C and O individual adsorption, correspondingly.

Subsequently, CO dissociation on the three selected bimetallic surfaces is calculated. The energy barriers, reaction energies, and geometries of transition states are presented in Figure 5(a)–(c). It is obvious that CO dissociation barriers strongly depend on the geometrical distribution of Ni ensembles. Namely, the highest one (3.87 eV) is obtained on the Ni monomer, followed by that on the Ni dimer, 3.20 eV, and the lowest is observed on Ni trimer- α , 3.01 eV. In the TSs, C atoms are almost located at a near bridge site, while the O atom almost sits at an hcp on CuNi-a, fcc on CuNi-c, and bridge on CuNi-d. The C–O bond lengths in corresponding TSs are 2.00, 1.95, and 1.91 Å, respectively, which are all apparently elongated relative to those in the ISs. The dissociation on the three surfaces is still endothermic with respect to CO molecular adsorption, and the reaction energies gradually decrease from Ni monomer to trimer- α , 2.96, 2.53, and 1.97 eV, respectively.

It is shown that the activation barrier as well as the reaction barrier on CuNi-a are as high as that on pure Cu(111), implying that CO activation on the Ni monomer is still unfavorable both thermodynamically and kinetically. In fact, coadsorption of C and O on the Ni monomer is stabilized. However, the stabilization is offset by the enhancement of CO molecular adsorption on the Ni monomer, and therefore, a comparable barrier is obtained. On the contrary, the C–O bond scission barriers are remarkably reduced on the Ni dimer and trimer- α and very close to the value on pure Ni(111). This indicates that the Ni dimer and trimer can dramatically enhance the activity toward CO activation. The promotion effects of the Ni dimer and trimer are attributed to the electronic and ensemble effects. For instance, the calculated d -band center of the Cu atom adjacent to the Ni dimer (CuNi-c) shifts upward to -2.43 eV from -2.56 eV on pure Cu(111) with respect to the Fermi levels. It is demonstrated in Figure 3 that the d -band center shifts up according to the content of Ni atoms increasing from dimer, trimer- α , to a whole Ni layer on the surface (CuNi-f). C atomic adsorption is enhanced more remarkably than that of CO, and thus the reaction energies are apparently lowered on dimer and trimer- α decorated Cu(111). Consequently, smaller barriers for C–O bond breaking are observed.

Moreover, it can be extrapolated that the values will be further decreased on ensemble with higher Ni content, such as CuNi-f. These findings agree well with the observation that the undesired methane yield increases as Ni content increases in CuNi catalysts.²²

It has been shown⁵² that for all the essential bond breaking reactions (e.g., C–O bond breaking) on metal surfaces the relation between reaction barriers and the reaction energies are almost linear. Meanwhile, it was found that CO dissociation barriers also correlate linearly with the coadsorption energies of C and O at the final states.⁵³ These are so-called Brønsted–Evans–Polanyi (BEP) relations: the lower the C+O coadsorption energy at the final state, the lower the CO dissociation barrier. From Tables 1 and 2, we found that the binding energies of C+O are much larger than those of H+OH, and the adsorption energy increments of C+O with increasing Ni concentration are also much more remarkable. This suggests that the effects of Ni-induced enhancement of C+O coadsorption as well as CO dissociation are much more evident. For example, the barrier of CO dissociation on the Ni trimer is almost 1 eV relative to that on Cu(111), and the value is nearly twice of that for H₂O dissociation. Of note, on CuNi-a, the stabilization of C+O coadsorption may be just offset by the enhancement of CO molecular adsorption, and therefore, a barrier for CO dissociation similar to that on Cu(111) is obtained.

In addition, it has been demonstrated by the *d*-band model that the step or kink sites with lower coordination would bind with atoms, such as C and O, much more tightly than the (111) surface.⁵¹ The coadsorption of C+O should certainly be enhanced at steps and kinks and would be further enhanced by Ni additives at steps or kinks. It can be expected that the further enhancement of C+O coadsorption energy would become more remarkable with increasing Ni loading. According to the BEP relations, smaller barriers of CO dissociation would be obtained as Ni concentration increases at steps and kinks. Ultimately, the dissociation of CO as well as the undesired methanation seem to be facilitated, but the process remains endothermic and with a large activation barrier. Further calculations on steps and kinks are required to confirm these expectations.

Through the investigation of H₂O and CO dissociations on the bimetallic surfaces, one can clearly see that Ni additives can promote the rate-limiting step, H₂O dissociation. This may be responsible for the Ni-enhanced WGS activity. Nonetheless, the promotional effects on CO dissociations also become more remarkable with increasing Ni loading. It can be deduced that the selectivity of the Cu–Ni bimetallic catalysts would decrease as Ni concentration increases, consistent with the experimental results.²² Finally, in real WGS catalyst designs, the oxide support is important and still necessary.⁵⁴ On the basis of the periodic slab model, our results have shown that the introduction of a moderate amount of Ni into Cu can enhance water dissociation (the rate-limiting step), therefore contributing to the whole WGS process. The results may be extrapolated to the supported Cu nanoparticles, suggesting that the reactivity toward WGS of the oxide-supported bimetallic CuNi nanoparticles with highly dispersed Ni ensembles containing lower Ni concentration may be superior to the monometallic Cu ones.

4. CONCLUSIONS

H₂O and CO dissociation are studied on a series of CuNi bimetallic surfaces by density functional theory to explore the

optimal ensemble with high reactivity toward the rate-limiting step in WGS but low reactivity toward CO activation. It is found that H₂O dissociation can be remarkably promoted on either the Ni monomer or other Ni ensembles with higher Ni content in the surface layer and hardly affected by the subsurface Ni. Furthermore, a good linear correlation is obtained between H₂O dissociation barriers and H adsorption energies: the larger the adsorption energy, the smaller the dissociation barrier. The promotional effects should originate from the Ni additive induced electronic and ensemble effects and understood through the *d*-band model. For the reaction pathway on CuNi, water dissociation is more practical via the dissociated H* rather than OH approaching Ni atoms.

As for CO dissociation on the three selected CuNi surfaces (Ni monomer, dimer, and trimer- α), the reaction barrier on the Ni monomer is found to be as high as that on pure Cu(111), implying C–O breaking on the Ni monomer is still unfavorable. In contrast, CO dissociation on the Ni dimer and trimer- α is promoted obviously, and the calculated barriers are very close to that on pure Ni(111). Thus, it is inferred that the Ni-induced promotional effects on C–O bond breaking would become more evident and ultimately facilitate the undesired methane yield with increasing Ni loading.

Conclusively, we suggested that Cu–Ni bimetallic catalysts with highly dispersed Ni ensembles containing lower Ni concentration may have relatively better activity and selectivity toward WGS.

AUTHOR INFORMATION

Corresponding Author

*Tel.: +86-20-87110426. Fax: +86-20-87112837. E-mail: zhaoyj@scut.edu.cn.

ACKNOWLEDGMENT

This work is supported by MOST under project 2010CB631302 and the Fundamental Research Funds for the Central Universities, SCUT, under projects 2009ZZ0068, 2011ZG0017, and 2011ZM0090, and completed with the cooperation of HPC Lab, Shenzhen Institute of Advanced Technology, CAS, China.

REFERENCES

- (1) Navarro, R. M.; Pena, M. A.; Fierro, J. L. G. *Chem. Rev.* **2007**, *107*, 3952–3991.
- (2) Huang, S.-C.; Lin, C.-H.; Wang, J. H. *J. Phys. Chem. C* **2010**, *114*, 9826–9834.
- (3) Gokhale, A. A.; Dumesic, J. A.; Mavrikakis, M. *J. Am. Chem. Soc.* **2008**, *130*, 1402–1414.
- (4) Knudsen, J.; Nilekar, A. U.; Vang, R. T.; Schnadt, J.; Kunkes, E. L.; Dumesic, J. A.; Mavrikakis, M.; Besenbacher, F. *J. Am. Chem. Soc.* **2007**, *129*, 6485–6490.
- (5) Fajin, J. L. C.; Cordeiro, M. N. D. S.; Illas, F.; Gomes, J. R. B. *J. Catal.* **2009**, *268*, 131–141.
- (6) Jelic, J.; Meyer, R. J. *J. Catal.* **2010**, *272*, 151–157.
- (7) Rodriguez, J. A.; Ma, S.; Liu, P.; Hrbek, J.; Evans, J.; Perez, M. *Science* **2007**, *318*, 1757–1760.
- (8) Liu, Z.-P.; Jenkins, S. J.; King, D. A. *Phys. Rev. Lett.* **2005**, *94*, 196102.
- (9) Senanayake, S. D.; Evans, J.; Agnoli, S.; Barrio, L.; Chen, T. L.; Hrbek, J.; Rodriguez, J. A. *Top. Catal.* **2011**, *54*, 34–41.
- (10) Barrio, L.; Kubacka, A.; Zhou, G.; Estrella, M.; Martinez-Arias, A.; Hanson, J. C.; Fernandez-Garcia, M.; Rodriguez, J. A. *J. Phys. Chem. C* **2010**, *114*, 12689–12697.

- (11) Ovesen, C. V.; Clausen, B. S.; Hammershøj, B. S.; Steffensen, G.; Askgaard, T.; Chorkendorff, I.; Norskov, J. K.; Rasmussen, P. B.; Stoltze, P.; Taylor, P. J. *Catal.* **1996**, *158*, 170–180.
- (12) Azzam, K. G.; Babich, I. V.; Seshan, K.; Lefferts, L. *Appl. Catal., B* **2008**, *80*, 129–140.
- (13) Rodriguez, J. A. *Prog. Surf. Sci.* **2006**, *81*, 141–189.
- (14) Gan, L. Y.; Zhang, Y. X.; Zhao, Y. J. *J. Phys. Chem. C* **2010**, *114*, 996–1003.
- (15) Schumacher, N.; Boisen, A.; Dahl, S.; Gokhale, A. A.; Kandoi, S.; Grabow, L. C.; Dumesic, J. A.; Mavrikakis, M.; Chorkendorff, I. *J. Catal.* **2005**, *229*, 265–275.
- (16) Callaghan, C. A.; Vilekar, S. A.; Fishtik, I.; Datta, R. *Appl. Catal., A* **2008**, *345*, 213–232.
- (17) Bian, J.; Xiao, M.; Wang, S. J.; Lu, Y. X.; Meng, Y. Z. *Catal. Commun.* **2009**, *10*, 1529–1533.
- (18) Vizcaino, A. J.; Carriero, A.; Calles, J. A. *Int. J. Hydrogen Energy* **2007**, *32*, 1450–1461.
- (19) Choi, Y. H.; Lee, W. Y. *J. Mol. Catal. A: Chem.* **2001**, *174*, 193–204.
- (20) Perez-Hernandez, R.; Galicia, G. M.; Anaya, D. M.; Palacios, J.; Angeles-Chavez, C.; Arenas-Alatorre, J. *Int. J. Hydrogen Energy* **2008**, *33*, 4569–4576.
- (21) Huang, T. J.; Yu, T. C.; Jhao, S. Y. *Ind. Eng. Chem. Res.* **2006**, *45*, 150–156.
- (22) Lin, J. H.; Biswas, P.; Gulians, V. V.; Mixture, S. *Appl. Catal., A* **2010**, *387*, 87–94.
- (23) Bezemer, G. L.; Bitter, J. H.; Kuipers, H.; Oosterbeek, H.; Holewijn, J. E.; Xu, X. D.; Kapteijn, F.; van Dillen, A. J.; de Jong, K. P. *J. Am. Chem. Soc.* **2006**, *128*, 3956–3964.
- (24) Ma, X. F.; Su, H. Y.; Deng, H. Q.; Li, W. X. *Catal. Today* **2011**, *160*, 228–233.
- (25) Andersson, M. P.; Abild-Pedersen, E.; Remediakis, I. N.; Bligaard, T.; Jones, G.; Engbæk, J.; Lytken, O.; Horch, S.; Nielsen, J. H.; Sehested, J.; Rostrup-Nielsen, J. R.; Norskov, J. K.; Chorkendorff, I. *J. Catal.* **2008**, *255*, 6–19.
- (26) Vendelbo, S. B.; Johansson, M.; Mowbray, D. J.; Andersson, M. P.; Abild-Pedersen, F.; Nielsen, J. H.; Norskov, J. K.; Chorkendorff, I. *Top. Catal.* **2010**, *53*, 357–364.
- (27) Kresse, G.; Hafner, J. *Phys. Rev. B* **1993**, *47*, 558–561.
- (28) Kresse, G.; Hafner, J. *Phys. Rev. B* **1993**, *48*, 13115–13118.
- (29) Kresse, G.; Furthmüller, J. *Comput. Mater. Sci.* **1996**, *6*, 15–50.
- (30) Kresse, G.; Furthmüller, J. *Phys. Rev. B* **1996**, *54*, 11169–11186.
- (31) Blöchl, P. E. *Phys. Rev. B* **1994**, *50*, 17953–17979.
- (32) Kresse, G.; Joubert, D. *Phys. Rev. B* **1999**, *59*, 1758–1775.
- (33) Perdew, J. P.; Yue, W. *Phys. Rev. B* **1986**, *33*, 8800–8802.
- (34) Perdew, J. P.; Chevary, J. A.; Vosko, S. H.; Jackson, K. A.; Pederson, M. R.; Singh, D. J.; Fiolhais, C. *Phys. Rev. B* **1992**, *46*, 6671–6687.
- (35) Kittel, C. *Introduction to Solid State Physics*, 6th ed.; Wiley: NY, 1986.
- (36) Henkelman, G.; Uberuaga, B. P.; Jonsson, H. *J. Chem. Phys.* **2000**, *113*, 9901.
- (37) Ahmed, J.; Ramanujachary, K. V.; Lofland, S. E.; Furiato, A.; Gupta, G.; Shivaprasad, S. M.; Ganguli, A. K. *Colloids Surf., A* **2008**, *331*, 206–212.
- (38) Pang, X. Y.; Xue, L. Q.; Wang, G. C. *Langmuir* **2007**, *23*, 4910–4917.
- (39) An, W.; Zeng, X. C.; Turner, C. H. *J. Chem. Phys.* **2009**, *131*, 174702.
- (40) Fajin, J. L. C.; Cordeiro, M. N. D. S.; Illas, F.; Gomes, J. R. B. *J. Catal.* **2010**, *276*, 92–100.
- (41) Phatak, A. A.; Delgass, W. N.; Ribeiro, F. H.; Schneider, W. F. *J. Phys. Chem. C* **2009**, *113*, 7269–7276.
- (42) Wang, G.-C.; Tao, S.-X.; Bu, X.-H. *J. Catal.* **2006**, *244*, 10–16.
- (43) Pallassana, V.; Neurock, M.; Hansen, L. B.; Norskov, J. K. *J. Chem. Phys.* **2000**, *112*, 5435.
- (44) Takenaka, S.; Shimizu, T.; Otsuka, K. *Int. J. Hydrogen Energy* **2004**, *29*, 1065–1073.
- (45) Hu, B.; Yamaguchi, Y.; Fujimoto, K. *Catal. Commun.* **2009**, *10*, 1620–1624.
- (46) Li, T.; Bhatia, B.; Sholl, D. S. *J. Chem. Phys.* **2004**, *121*, 10241.
- (47) Lee, K.; Song, C.; Janik, M. J. *Appl. Catal., A* **2010**, *389*, 122–130.
- (48) Liu, Z. P.; Hu, P. J. *Am. Chem. Soc.* **2003**, *125*, 1958–1967.
- (49) Liu, X. M.; Lu, G. Q.; Yan, Z. F.; Beltramini, J. *Ind. Eng. Chem. Res.* **2003**, *42*, 6518–6530.
- (50) Blyholder, G. J. *Phys. Chem.* **1964**, *68*, 2772.
- (51) Hammer, B.; Nørskov, J. K. *Adv. Catal.* **2000**, *45*, 71–129.
- (52) Wang, S.; Temel, B.; Shen, J.; Jones, G.; Grabow, L. C.; Studt, F.; Bligaard, T.; Abild-Pedersen, F.; Christensen, C. H.; Norskov, J. K. *Catal. Lett.* **2011**, *141*, 370–373.
- (53) Liu, Z. P.; Hu, P. J. *J. Chem. Phys.* **2001**, *114*, 8244.
- (54) Park, J. B.; Graciani, J.; Evans, J.; Stacchiola, D.; Senanayake, S. D.; Barrio, L.; Liu, P.; Sanz, J. F.; Hrbek, J.; Rodriguez, J. A. *J. Am. Chem. Soc.* **2010**, *132*, 356–363.